PERGAMON

Solid-State Electronics 45 (2001) 831–840

SOLID-STATE ELECTRONICS

Photon assisted field emission from a silicon emitter

K.L. Jensen [a,*], Y.Y. Lau [b], D. McGregor [b]

[a] *Naval Research Laboratory, Code 6841, Electronic Science and Technology Division (ESTD), Vacuum Electronics Branch, Washington, DC 20375-5347, USA*

[b] *Nuclear Engineering and Radiation Science, University of Michigan, Ann Arbor, MI 48109-2104, USA*

Abstract

A novel method for the high-frequency modulation of a semiconductor field emitter array (FEA), as needed by compact high power microwave and millimeter wave tubes, is qualitatively analyzed. The model examines a FEA held at the threshold of emission by an applied gate potential from which current pulses are triggered by the application of a laser pulse on the backside of the semiconductor. Such an arrangement produces electron bunches ("density modulation") at GHz frequencies without suffering from the restriction in reduced emission area and small unit cell geometry imposed by the high capacitance of field emitters. The analysis proceeds by first developing an analytical model of the emission from a silicon tip using a modified WKB approach to the tunneling current, which is validated by the more exact Airy function approach to solving Schrödinger's equation. The effects of band bending are explicitly accounted for. The resulting relations are used to estimate emission from a single hyperbolic structure, and generalized to an array where a distribution in tip radii and work function is possible. Using a simple relationship between the incident photon flux and the resultant electron density at the emission site, an estimation of the tunneling current is made. Finally, a brief description of the operation and design of such a "photon-assisted field emission device" is given.

1. Introduction

In comparison to solid state devices, microwave power tubes provide higher power operation with larger currents, higher threshold for voltage breakdown, and increased bandwidth due to the higher electron mobility in vacuum [1,2]. Amplifiers under development for communications, electronic warfare, and radar would benefit in several ways from advances in electron source technology. First, to meet high current density requirements in the beam tunnel, thermionic sources require focusing magnets to create beam-area convergence ratios exceeding 10:1 so that sufficiently high current densities are achieved in the beam tunnel, but this in turn requires sophisticated electron gun designs using highly convergent magnetic fields. Relaxing beam convergence demands would reduce the complexity of the magnetic field profile and relax the machining tolerances required to avoid interception from beam scalloping. Second, much of the circuit of a typical TWT or Klystron is used to prebunch the electron beam prior to power extraction: shortening the circuit would reduce the size of the magnets needed and therefore reduce the weight and volume of the amplifier (and, possibly, the power consumption). Third, uniformity of emission is critical: a laminar and uniform beam results in the best beam transport for the least magnetic field and reduces losses to the tube walls. Likewise, reduced emittance electron beams (caused by non-uniform emission and thermal velocities at the source, as well as non-axisymmetric current density) are also critical for amplifier performance, but also for design: uniform beams are typically presumed in simulations to ease computational complexity. And finally, to extend lifetime, typical thermionic cathodes are typically operated at 0.5–1 A/cm^2 (but occasionally as high as 5 A/cm^2, or for short pulses up to 100 A/cm^2). Elevating the cathode temperature allows operation at higher current densities but

* Corresponding author. Tel.: +1-202-767-3114; fax: +1-202-767-1280.

E-mail addresses: kevin.jensen@nrl.navy.mil, jensen2@estd.nrl.navy.mil (K.L. Jensen).

0038-1101/01/$ - see front matter
PII: S0038-1101(01)00055-7

at the price of operational lifetime due to the more rapid evaporation of the low work function coating required for efficient operation (e.g., barium in a dispenser cathode): using a (fixed temperature) theoretical model with generic parameters [3], raising the cathode temperature by 100°C correlates with a reduction in lifetime to a quarter of the original lifetime. In practice, an increase in operational temperature is required to maintain the current density, so lifetimes are shorter: when changing the operating current density from 1 to 5 A/cm^2 (corresponding to $T \approx 1000$ and 1100°C for a work function of 2.13 eV in Richardson's equation), the lifetime for an M-type cathode drops by a factor of 1/30, and a B-type cathode by a factor of 1/10 [4]. [1]

Field emitter arrays (FEAs) offer solutions to the aforementioned limitations of thermionic cathodes for a variety of devices, but in particular, advanced microwave power amplifiers, by virtue of their high current density and high pulse repetition frequencies [5]. Dramatic improvements in amplifier performance are enabled by density modulation the electron beam [6–8], because the beam's kinetic energy can then be transferred more efficiently to an rf field. RF amplifiers at present rely on the interaction of an electron beam with the slow wave supported by the circuit ("velocity modulation") to prebunch electrons prior to the extraction of the beam energy by rapid deceleration of the electron bunch. It has long been recognized that if the electron beam could be bunched at the cathode surface itself, then the substantial portion of the interaction circuit (approximately 80% for a helix-TWT) would thereby be eliminated [9], substantially reducing the overall dimensions of, e.g., vacuum power boosters presently used in microwave power modules. Reductions in device weight through the elimination of the premodulation circuit are enabled. Consequently, the most significant impact that the FEA would have on vacuum microwave devices is to produce an electron beam modulated at microwave frequencies. In fact, based on the good performance of FEAs in a recent FEA–TWT demonstration and on simulation, Whaley et al. conclude that "potential for high-frequency modulation and the benefits that it will provide ... make the FEA–TWT an attractive microwave amplifier alternative with performance not achievable with a conventional thermionic TWT [10]".

Density modulation of the electron beam, however, carries a cost. At the beginning of the ARPA/NASA/NRL (Klystrode) and NRL (Twystrode) programs in 1994, four challenges were identified: (i) to design a tube that was compatible with the FEA, (ii) to overcome the initial transverse velocity produced at the FEA and form a usable electron beam, (iii) to develop a matching network to efficiently couple rf fields into the low impedance FEA structure, and (iv) to produce stable, copious emission at high current density in a tube environment [11–13]. At the conclusion of both programs in 1997, while the first three goals had been met, the last had not due to premature FEA failure due to arcing in the power tube at current levels two orders of magnitude smaller than design requirements; even in the controlled environment of test stations, maximum currents obtained were nevertheless still an order of magnitude too small [14]. A variety of factors contributed, but in particular, because of the high-frequency (10 GHz) modulation of the gate potential and the inherent FEA capacitance, the FEA ring cathodes were of small emission area and resistive protection was precluded. Hence, the individual emitters were driven hard but were not protected against arc damage.

In the following, we shall describe an alternate method for producing electron bunches by optical means. A brief description of the mechanisms involved and the advantages that are obtained shall be given. The majority of the work shall be devoted to providing a fundamental description of the mechanism by which electrons are emitted from a semiconductor surface. A modified form of the Fowler–Nordheim equation (FNE), including band bending and electron exchange-correlation potential effects on the field emission process, shall be advanced and validated by comparison to an exact Airy function solution to Schrödinger equation for the evaluation of the transmission coefficient. Finally, a qualitative estimation of array performance, and an indication of impact on device performance will be given.

2. Optical modulation of a field emitter

Achieving density modulation without gate modulation would significantly relax requirements on FEA performance. If a semiconductor FEA is held at the threshold of emission by an applied gate potential, current pulses can be generated by the application of a laser pulse on the backside of the semiconductor, as in Fig. 1. Density modulation can then be achieved at GHz frequencies without suffering from the restriction in reduced emission area and small unit cell geometry. Such an arrangement shall be designated photo assisted field emission device (PAFED) [15]. Bypassing gate modulation has many advantages. The capacitance limitation that constrained the development of field-emitter-based power tubes can be circumvented. Risk of arc damage is reduced, since electron emission is triggered optically, allowing the gate potential to remain at reduced values. Increased gain of the amplifier results due to the elimination of power consumed to drive the gate potential at

[1] Fig. 5.27 of Ref. [1].

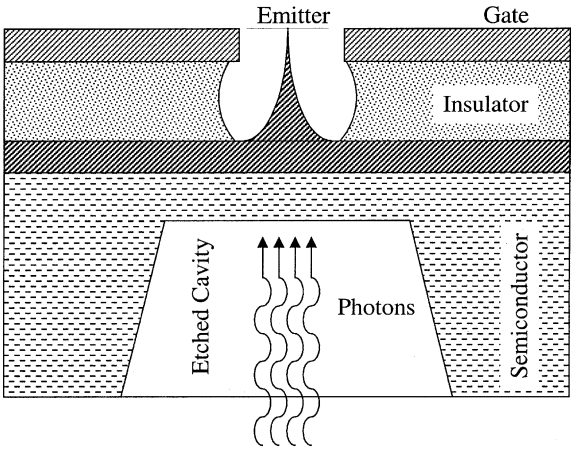

Fig. 1. Schematic diagram of PAFED (not drawn to scale).

GHz frequencies. Standard resistive protection schemes may be utilized to protect FEAs against arc damage. Increased emission area, due to bypassing the capacitance limitations on gate modulation, results in a reduced tip load (current per tip) on the field emitters, further reducing the risk of arc damage. Tailored harmonics through adjustments in the bias voltage and/or laser intensity allow tremendous flexibility in frequency, pulse shaping, and level of emission. Ease of thermal management is enabled by forced convection cooling applied through a carrier gas that flows between the optical light source and the device backside. And finally, integrated functionality of Si in the microelectronics industry allows for combining various integrated devices with the PAFED.

Typical field emitters operate through the generation of very high fields at the apex of a sharpened emitter structure. The potentials which generate the high fields are obtained from a gate at close proximity to the emitter tip, usually coplanar with the apex and on the order of a micron in diameter. For large enough voltages, the strong fields at the apex of the emitter make the barrier to electron emission so narrow that electrons may quantum mechanically tunnel through the barrier and escape. The relationship between the field at the apex (which is proportional to the gate potential) and the emitted current is typically represented as:

$$I_{\text{anode}}(V_g) = A_{\text{FN}} V_g^2 \exp(-B_{\text{FN}}/V_g) \tag{1}$$

where V_g is the gate potential and A_{FN} and B_{FN} are constants dependent upon emitter geometry and work function. Because of the exponential dependence of current upon gate potential, a sinusoidal modulation of the gate potential, as in $V_g(t) = V_{dc} + V_{rf}\sin(\omega t)$, produces narrow bunching. However, because of the capacitance of the field emitter, power is therefore required to drive the cathode, typically on the order of a few watts [16]. A reduction in drive power entails an increase in the gain of the amplifier. In PAFED, the gate potential is held at a value just below the onset of significant electron emission. Significant field emission current is triggered when the backside of the device is illuminated by LED or laser diode. Optically controlling field emission provides ready modulation of field emitters at GHz and beyond. A high resistivity semiconductor such as Si, whose conductivity and the quasi-Fermi level can be changed through the photoconductive effect, in which absorbed photons excite electrons from the valence band to the conduction band, is utilized. The increase in electron density in the conduction band of the Si field emitter tip will locally change the work function of the material, thereby causing the tip to change from its previous non-emitting condition to an electron emission condition, as the field emitter is almost on the verge of field emission by the DC bias. The DC biased electric field, combined with electron diffusion, will promote the drift of the excited electrons towards the field emitter tips.

3. Field emission from a semiconductor

3.1. Fowler–Nordheim theory

The canonical model for field emission from a metal represents the material-metal interface as a step-function barrier of height V_0 (eV) subject to an applied field $eE \equiv F$ (eV/Å). The transmission coefficient $T(k)$ of an incident electron is defined as the ratio of the transmitted to incident current densities $J_{\text{trans}}/J_{\text{inc}}$. The total current density is obtained by integrating the product $T(k)$ with the supply of electrons $f_0(k)$ (#/Å^2) and the electron velocity $v(k) = \hbar k/m$ (Å/fs). For a barrier of height $V_0 = \phi + \mu$, where ϕ (eV) is related to the work function [18] and μ (eV) is the chemical potential [19], the solution to $T(k)$ is given in terms of Airy functions, but for typical fields, asymptotic expansions [20] may be used which are equivalent to the WKB solution [21]

$$T_\Delta(k) = \exp\left\{ -\frac{4\sqrt{2m\phi}}{3\hbar F}(V_0 - E(k))^{3/2} \right\} \tag{2}$$

where the terms are as listed in Tables 1 and 2 and Appendix A. Image charge modifications, due to many-body exchange-correlation potentials [22–26], introduce an additional term to the linear potential such that $V(x) = V_0 - Fx - Q/x$. The image term lowers the barrier by $\sqrt{(4QF)}$ and reduces its width such that a net increase in electron transmission by up to two orders of magnitude results. Including (Q/x) is tantamount to

Table 1
Fundamental terms and constants (eV, Å, fs, $q = 1$)

Symbol	Definition	Formula	Value
m_0	Electron rest mass	–	510998.9 eV/c^2
$\hbar$	Planck's constant/2π	h/2π	0.6582119 eV fs
c	Speed of light	–	2997.925 Å/fs
q	Electron charge	–	1
ε_0	Permittivity of free space	$q^2/4\pi\alpha\hbar c$	5.526350×10^{-3} q^2/eV Å
α	Fine structure constant	–	1/137.036
a_0	Bohr radius	$\hbar/\alpha m_0 c$	0.5291772 Å
k_B	Boltzmann's constant	–	8.617341×10^{-5} eV/K

Table 2
Material parameters for silicon and molybdenum at $T = 300$ K

Symbol	Description	Silicon	Molybdenum
M_c	Conduction band eqv. minima	6	1
Φ	Experimental work function	$\chi - \mu$	4.41 eV
χ	Electron affinity	4.05 eV	$\mu + \Phi$
ρ_0	Bulk electron density	10^{-6} #/Å^3	0.06463752 #/Å^3
μ_0	Bulk chemical potential	–0.08611525 eV	5.873 eV
Q	$\alpha\hbar c(K_s - 1)/4(K_s + 1)$	3.041785 eV Å	3.599911 eV Å
m	Electron effective mass	$0.3282800 m_0$	m_0
K_s	Dielectric constant	11.9	$\gg 1$
N_c	Density coefficient	2.831983×10^{-5} #/Å^3	2.509416×10^{-5} #/Å^3

inserting two functions $v(y)$ and $t(y)$ [27] [2] in the coefficients of ϕ and $(E(k) - \mu)$, respectively, in a Taylor expansion of $-\ln(T_\Delta(E(k)))$ to first order in $(E(k) - \mu)$, where $y = \sqrt{(4QF)}/\phi$:

$$T_{\mathrm{LWKB}}(k) = \exp\left\{ -\frac{4\sqrt{2m\phi}}{3\hbar F}\left(\phi v(y) - \frac{3}{2}t(y)[E(k) - \mu]\right)\right\} \tag{3}$$

where the subscript "LWKB," short for linearized WKB, indicates that the argument of the exponential is Taylor expanded to first order (linear) in energy, as used in the derivation of the FNE. The expansion point for the FNE is about μ. Integrating Eq. (3) with the supply function $f_0(k)$ results in

$$J(F) = a_{\mathrm{fn}} F^2 \mathrm{e}^{-b_{\mathrm{fn}}/F}\left[\frac{\pi c_{\mathrm{fn}}}{\beta \sin\left(\frac{\pi c_{\mathrm{fn}}}{\beta}\right)} - \left(1 + \mu c_{\mathrm{fn}} - \frac{c_{\mathrm{fn}}^2}{\beta^2} g\right) \times \exp(-\mu c_{\mathrm{fn}})\right] \tag{4}$$

where a_{fn}, b_{fn}, c_{fn}, and g are field- and work-function dependent terms (see Appendix A). [3]

For field emission from metals, the $\exp(-\mu c_{\mathrm{fn}})$ term is typically negligible: for molybdenum parameters given in Table 2 and an applied field of 0.5 eV/Å, the magnitude of the first and second terms are 1.023144 and 1.913137×10^{-6}, respectively; in fact, for metals, g is of no account due to the magnitude of $\beta\mu$. However, for silicon-like parameters, the second term in Eq. (5) can be a non-trivial percentage of the first depending upon the applied field and the chemical potential, though g remains negligible at fields of interest.

For metals, it is adequate to approximate ϕ by the work function Φ and the chemical potential μ by E_F because the zero-temperature limit of μ is equal to the Fermi energy, or

$$\mu \approx \mu_0 \equiv E_F = \frac{\hbar^2}{2m}\left(3\pi^2\rho\right)^{2/3} \tag{5}$$

where $\mu_0 = \mu$ ($T = 0$ K), and where ρ is the density of electrons in the "free electron Fermi gas" approximation

[2] An extensive discussion of these functions and methods to calculate them can be found in Ref. [27].

[3] Notation follows Eq. (C1) of Refs. [25,26] with the identification $c_{\mathrm{fn}} = \beta\zeta/\pi$; an error in parenthesis (also occurring in Ref. [5]) has been corrected so that agreement with Ref. [20] results.

[28]. These approximations are adequate due to the large value of ρ for metals, as in Table 2, which serve to shield the interior of the metals from applied electric fields and render the chemical potential temperature independent to a good approximation, that is, $(\mu - \mu_0)/\mu_0 \approx 3(\pi/6\beta\mu_0)^2 \ll 1$ [19]. The electron density in bulk semiconductors is orders of magnitude smaller, indicating that the chemical potential must be treated much more carefully, applied electric fields are not shielded as effectively (band bending at the surface occurs), and the derivation of Eq. (5) needs to be revisited. We consider each of these in turn.

3.2. The chemical potential

The electron density in a semiconductor can be calculated from the Fermi–Dirac distribution function [29]

$$\rho(x) = 4\frac{M_c}{\sqrt{\pi}}\left(\frac{m}{2\pi\beta\hbar^2}\right)^{3/2}\int_0^\infty \frac{\sqrt{y}\,\mathrm{d}y}{1+\mathrm{e}^{y-\beta\mu}} \equiv N_c\frac{2}{\sqrt{\pi}}F_{1/2}(\beta\mu(x)) \tag{6}$$

where M_c is the number of equivalent minima in the conduction band, $F_{1/2}(x)$ is the Fermi–Dirac integral, and where m is the effective mass of the electron (for silicon, the longitudinal and transverse effective masses are $0.98m_0$ and $0.19m_0$, respectively, so $m = (m_l m_t^2)^{1/3} \approx 0.328\ m_0$, as in Table 2). The electrochemical potential in Eq. (7) is given by $\mu(x) = \mu_0 + \varphi(x)$, where φ is the solution of Poisson's equation. The boundary conditions are that at the surface, $K_s\partial_x\varphi = F$ (F is the field in vacuum), where K_s is the dielectric constant; the absence of the negative sign is a reflection of the incorporation of the electron charge into V and F). For the fields characteristic of field emission, the following approximation may be used to relate the externally applied field to the electrochemical potential at the surface [30,31]:

$$F_{\mathrm{vac}}^2 = \frac{4\ N_c K_s}{\sqrt{\pi}\beta\varepsilon_0}\int_0^\infty \sqrt{y}\ln\left(1+\mathrm{e}^{\beta\mu-y}\right)\mathrm{d}y \approx \frac{2\pi^2 K_s N_c}{3\beta\varepsilon_0}\left(\frac{\beta\mu}{\pi}\right)^{1/2}\left[\frac{8}{5}\left(\frac{\beta\mu}{\pi}\right)^2+1\right] \tag{7}$$

When the applied field is specified, Eq. (7) is solved to obtain the electrochemical potential. μ is therefore a function of both applied field and temperature. The values of relevant silicon parameters at room temperature and for generic parameters are given in Table 2.

The estimation of field emission current from semiconductors may assume that the band bending due to an applied field can be calculated in the zero emitted current approximation (ZECA) [17,31], from which a chemical potential required in the supply function may be inferred. Simulations using a (Wigner) quantum distribution function approach have shown that at fields where tunneling becomes significant, ZECA overestimates the degree of band bending and therefore tunneling current. The density profile presumed by ZECA is not in fact valid near the semiconductor–vacuum interface [32], and this in turn is traceable to the wave nature of the electron (the de Broglie wavelength for an electron in bulk silicon with energy E is approximately $\hbar/\sqrt{(2mE)}$ and is on the order of a few angstroms). Consequently, the sharp rise in density presumed by the ZECA approach overestimates calculations of the chemical potential.

3.3. Image charge approximation

Self-consistent solutions of electron density profiles near metal–vacuum interfaces indicate, however, that a shifted image charge potential is warranted [33] and accounts for the conclusion (using a density gradient analysis) that the standard image charge approach to calculating current density overestimates the current density [34]. A departing electron will induce a charge distribution on the surface of a metal that gives rise to the image charge approximation. The classical image charge model remains valid to within a few angstroms from the surface. Closer than that, exchange-correlation potentials due to electron density variation cause deviations from the simple image charge form. Elsewhere, it was shown that for metals, the image charge potential resembles [25,26]

$$V(x) = \mu + \Phi_0 + \frac{8}{3\pi}Qk_F^3x_i^2 - F(x-x_0) - \frac{Q}{(x+x_0)} \tag{8}$$

where $x_0 = \hbar\sqrt{(2mV_{\max})}$, $V_{\max}$ is the maximum value of the potential, $\hbar k_F = \sqrt{(2m\mu)}$, and $x_i(k_F x_0)$ is the origin of the background positive charge. This suggested that the FNE could be retained by using an effective work function defined by

$$\Phi^* = \Phi_0 + \frac{8}{3\pi}Qk_F^3x_i^2 + 2Fx_0 \tag{9}$$

Eqs. (8) and (9) were considered for semiconductor parameters, but the smallness of μ at the surface resulted in an unrealistic x_0 parameter, such that no combination of parameters results in a fit to published experimental data considered below (a strong indication of the degree to which the parameters of the theory are constrained). Modifications to the standard image charge potential along the lines of Eqs. (8) and (9) will have to await a more refined treatment of the electron density in conjunction with band bending and related self-consistently to tunneling (e.g., the aforementioned Wigner function). In the absence of that study, the standard

image charge model with the dielectric modification (i.e., $Q \Rightarrow (K_s+1)Q/(K_s-1)$) shall be used, as is in common practice.

3.4. The WKB approximation

The surface chemical potential for silicon parameters provides an indication that standard WKB usage in the derivation of the FNE may require some modification by virtue of the possible smallness of $\beta\mu$ [20]. Complications manifest themselves on two issues: the second term in parentheses in Eq. (4) is no longer negligible (but nevertheless small), but more importantly, the derivation of the FNE [35] [4] chooses as the Taylor expansion point of $\ln(T(E))$ the value $E \approx \mu$. As seen in Fig. 2, using the expansion point $E \approx \mu$ shows deviations from exact results (Airy function approach [36]) The WKB form is given by [5]

$$-\ln(T_{\mathrm{WKB}}(k)) \equiv \theta(k) = \frac{2}{\hbar}\sqrt{2mFL^3}\; G\left(\frac{x_-}{L}\right) \tag{10}$$

where $x_\pm(E(k))$ are the zeros of the standard image charge potential and $L(E(k)) = x_+ - x_-$. The FN curve is calculated using the approximation that $v(y)$ is linear in y^2 in the derivation of the FNE, as is common practice. The smallness of the chemical potential poses a problem for both WKB and FN, as in either approximation, $T(k)$ does not vanish for small energy. As suggested by Fig. 2, the energy distributions will be incorrect. Greater correspondence to exact results is obtained through the introduction of an energy dependent coefficient [20], but for the parameters considered herein, resulting current density estimates made using Eq. (10) are within 30% of exact results. We conclude that for the analysis contained herein, the LWKB method is sufficiently rapid to allow for the iterative calculations to be performed with reasonable efficiency upon a desktop computer. The LWKB approximation will therefore be used in the calculation of the current density.

Because the effective mass of an electron in metals does not differ from the electron rest mass in vacuum, the distribution function in Eq. (A.2) may be integrated with the transmission coefficient to yield the tunneling current without further modification. For semiconductors, there is an effective mass discontinuity at the surface which complicates the analysis of transport through interfaces between different media (e.g., Ref. [37]). In view of the uncertainties incurred by the approximations used, a simpler approach will suffice. The distribution function used in the evaluation of the tunneling current shall be related to the distribution function in the semiconductor by equating the electron density as per $\rho(x=0^-) = \rho(x=0^+)$, which involves finding a chemical potential in vacuum such that (c.f. Eq. (6))

$$M_c m^{3/2} F_{1/2}(\beta\mu) = m_0^{3/2} F_{1/2}(\beta\mu_{\mathrm{vac}}) \tag{11}$$

The (vacuum) supply function $f_0(k)$, using μ_{vac}, is integrated with $v(k)T(k)$ to obtain the current density for tunneling through the (vacuum) image charge potential barrier.

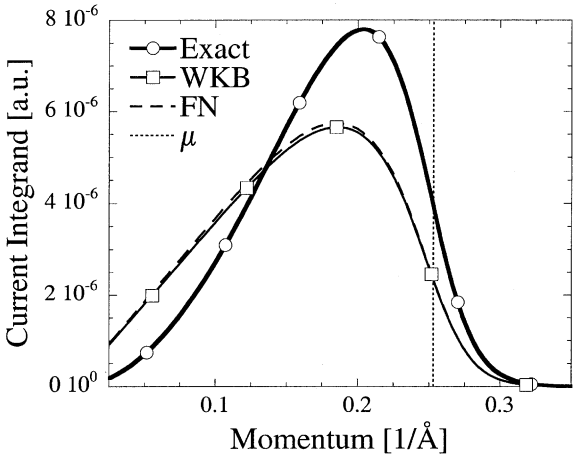

Fig. 2. Comparison of the various approximations to the current integrand $v(k)\,T(k)\,f_0(k)$ for $F = 0.5$ eV/Å. "Exact" is from Airy function simulations. "WKB" refers to Eq. (10). "FN" refers to Eq. (3). "μ" shows the Fermi momentum, which serves as the expansion point in the derivation of the FN equation.

3.5. Transition from 1-D to 3-D: gated hyperbolic semiconductor emitters

The "statistical hyperbolic model" of a field emitter [5,38] relates the field at the apex of an emitter to the gate potential by using a field enhancement factor such that $F_{\mathrm{tip}} = \beta_g V_g$, and the tip current to the current density on axis by use of an area factor such that $I_{\mathrm{tip}} = b_{\mathrm{area}} J_{\mathrm{FN}}(F_{\mathrm{tip}})$ in terms of the tip radius a_s, gate radius a_g, and cone angle β_c. The ratio of the array current to the product of the tip current with the number of emitters defines the statistical factor Σ. In addition to assuming a linear distribution in tip radii such that $a(s) = a_s(1+s)$, where $0 \leqslant s \leqslant \Delta s$, a linear distribution in effective work function such that $\Phi(s) = \Phi^* + s\Delta\Phi$ is invoked. The statistical factor becomes

[4] We shall follow the methodology of Forbes and Jensen [35].

[5] Derivation is given in Forbes et al. [35], but differences in notation occur.

$$\Sigma(V_g, \Delta s, \Delta\Phi) = \left(\frac{1-\exp(-b_a\Delta s)}{b_a\Delta s}\right)\left(\frac{1-\exp(-b_\phi\Delta\Phi)}{b_\phi\Delta\Phi}\right) \tag{12}$$

where b_a and b_ϕ are perforce numerically calculated using an Euler differencing scheme to approximate the derivatives $b_X = -\partial_s \ln(I_{tip}(X))$, where X is either $a(s)$ or $\Phi(s)$.

Comparison with experimental data is required to validate the claim of qualitative accuracy of the model. We have chosen to simulate data obtained by Temple et al., for silicon field emitters produced by MCNC. The following parameters were extracted from $I(V)$ data, reported parameters, and images of the field emitter apex [39]: [6] tip radius $= 25 \pm 5$ Å, gate radius $a_g = 0.9$ μm, apex half angle $= 21° \pm 2°$, and number of emitters $=$ 18291. Given the uncertainty, values of $a_s = 26$ Å and hyperbolic cone half angle $\beta_0 = 20°$ were found to be optimal. All other parameters not specified are assumed to be typical of silicon, as in Fig. 1. We ignore the thickness of any oxide on the emitter, and therefore do not consider tunneling through the oxide, though such related issues are likely to be important [40]. In the experimental data a 100 kΩ gate resistor was incorporated to protect against arc damage to the gate. It produces effects analogous to, but not equivalent to, lateral resistors used to protect arrays [41]. Finally, parameters not explicitly specified are assumed to be standard silicon parameters.

Under normal FEA operation, some gate current is inevitable, and is typically on the order of 0.5% when conditions are well away from the Child's Law (space charge) limit. A qualitative calculation shows that under present circumstances for a gate voltage of 75 V, the anode current is small (but nevertheless non-trivial) fraction of the space charge limit: a rise in gate current may be anticipated due to a greater proportion of electrons turned around to, and intercepted by, the gate. The degree of current interception is, at this stage, an ad hoc assumption. Below, it is assumed that 0.85% of the anode current is intercepted by the gate at the upper voltage regime, thereby giving rise to an IR voltage drop. The $I(V)$ curves with and without this correction are shown in Fig. 3. The effect R is to cause the $I(V)$ curve at higher voltages to become less exponential and more linear, as V_g is replaced by $V_g + I_{gate}R$ in Eq. (1). The statistical factors Δs and $\Delta\Phi$ are taken as 0.2 and 0.3 eV, respectively: the former is typical, but can be adjusted for a better fit to experiment, and the latter is obtained by assuming an 80% reduction in current over time from initial "clean" values. With such values, $\Sigma(V, \Delta s, \Delta\Phi)$ varies between 27% for low voltages up to 35% for high voltages. Given the simplicity and limitations of the model, the agreement with experimental data from MCNC is surprisingly good, and demonstrates the qualitative utility of the theoretical effort.

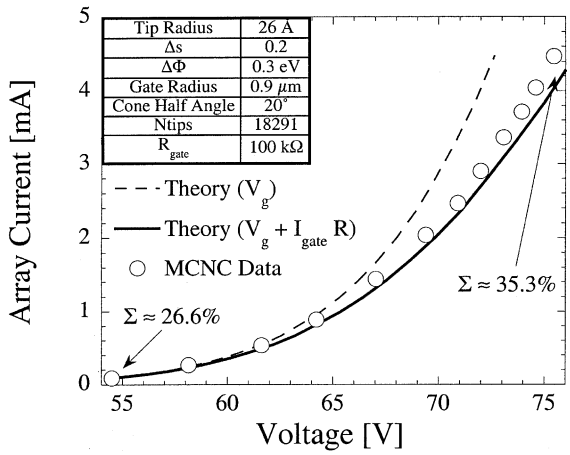

Fig. 3. Comparison of the semiconductor statistical hyperbolic model with linear variation in tip radius and work function with experimental data from Temple et al. [39] on a field emitter manufactured by MCNC. "Σ" refers to the statistical factor Eq. (12), which shows that as the voltage increases, the number of tips significantly contributing to the current increases. The dashed line is the current in the absence of any resistance.

3.6. Estimation of emission current due to laser pulse

Electron mobility values in silicon are on the order of 2000 cm^2/V s at room temperature [42], implying that the average time between collisions is on the order of 370 fs. For an electron of effective mass m and a kinetic energy of 0.356 eV, the distance traveled in that time is on the order of $d_\tau = 0.23$ μm (further in light of the strong electric fields present but neglected in this simple analysis). We therefore expect that electrons created by a laser pulse on the back side of the field emitter will travel to the apex of the emitter sufficiently fast to allow optical modulation at 10 GHz frequencies. Assuming a quantum efficiency of 0.76, a wavelength of 8400 Å ($E =$ 1.476 eV), and an exposure area of radius $R = 0.75$ μm, $P = 1$ MW/cm^2 laser will generate $N_l = 5679219$ electrons in a $\delta t = 0.1$ ns pulse with an energy above the conduction band in bulk of $E - E_g = 0.356$ eV, where $E_g = 1.12$ eV is the bandgap of silicon. If we assume that the electrons are uniformly distributed in a cone of

[6] The tip radius and hyperbolic cone half-angle were extrapolated from Fig. 4 of Ref. [39]. Gate radius and number of emitters were taken from the text and from Fig. 9 of Ref. [39]. The $I(V)$ data attributed to MCNC was interpolated from Fig. 9 of Ref. [39].

half-angle β_c and a height equal to d_τ, then the density is of the order

$$\delta\rho \approx \frac{N_l}{\frac{1}{3}\pi\, d_\tau^3 \tan^2(\beta_c)} \tag{13}$$

If the electrons crowd as they approach the apex, then the density would be larger; if they are spread out over a length scale larger than d_τ, then the density would be smaller. Eq. (13) is therefore an indication of the magnitude of $\delta\rho$. For the parameters quoted, Eq. (13) gives $\delta\rho = 0.002711$ #/Å^3. For fields of interest, $\beta\mu$ is sufficiently larger than unity so the Fermi–Dirac integral function may be reasonably approximated by its leading order term, from which

$$\mu_{\rm vac} \approx \frac{\hbar^2}{2m_0}\left(3\pi^2\rho\right)^{2/3} \tag{14}$$

and $\mu \approx \mu_{\rm vac}/rM_c^{2/3}$, where $r = (m/m_0)$. For silicon parameters, $\mu \approx 0.922546\mu_{\rm vac}$. Combining results, the rise in the chemical potential at the surface due to the laser pulse becomes

$$\mu' = \mu\left(1 + \frac{\delta\rho}{\rho}\right)^{2/3} \tag{15}$$

where the unprimed quantities are the values in the absence of the laser pulse.

In Fig. 4, the relationship between the array current and the chemical potential is shown for parameters used in Fig. 3, but assuming an emission disk of radius 1 mm with tips on a triangular lattice spaced 10 μm apart ($N_{\rm tips} = 72552$). [7] If the gate potential is held such that prior to the pulse the emission current is 0.1 mA ($\mu_{\rm vac} \approx 0.2194$ eV; $\rho \approx 0.0004749$ #/Å^3), then the estimate based on Eq. (15) using an unmodified Eq. (13) indicates that the pulse will cause the chemical potential to increase by a factor of 3.56. which extrapolates to a current level a factor of 10^6 larger than the initial current. If the length scale in Eq. (13) is, however, a factor of 2 larger than d_τ, then $\delta\rho$ would be a factor of 8 smaller, μ' a factor of 1.43 larger than μ, and hence the current level would be a factor of 300 larger than the initial current. It is not an unreasonable conclusion, therefore, that current pulses three orders of magnitude larger than the initial current are obtainable depending on the intensity of the laser and the gate voltage conditions corresponding to "turn on". Significantly, as shown by Whaley et al., [8] the modulation ratio $I_{\rm ave}/I_{\rm peak}$ does not have to be small to achieve good efficiency in an emission-gated TWT. Consequently, the capabilities implied by PAFED technology have significant promise.

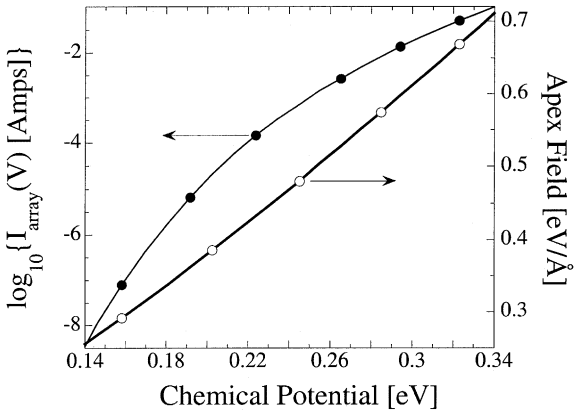

Fig. 4. Relation of array current to apex field and (vacuum) chemical potential (Eq. (11)) at the apex. Increases in the chemical potential occur as a consequence of a laser pulse.

4. Conclusion

We have endeavored to provide a qualitative description of the operation of a PAFED, and have shown that the mechanism may allow for the generation of current pulses that would be of significant utility in terms of efficiency and compactness for next generation TWTs relying on bunching of the electron beam at the cathode. To accomplish this analysis, a model of field emission from silicon was developed. The validity of various approximations in the ZECA used to estimate current from semiconductors were assessed. The one-dimensional model was validated against an Airy function solution of Schrödinger's equation, and its three-dimensional extension was compared favorably to experimental data. A numerical implementation of the model, using generic parameters, predicted that current pulses several orders of magnitude greater than the base-line current could be obtained, demonstrating that the PAFED concept has evident utility in the possible generation of electron bunches required by next generation microwave amplifier devices.

Acknowledgements

We thank Dr. Dorota Temple of the Microelectronics Center of North Carolina (MCNC) for permission to use her data (Ref. [39]).

[7] The present analysis updates and corrects the analysis of Jensen et al. [43].

[8] See Whaley, et al. in Refs. [8,10].

Appendix A. Table of mathematical functions

Name	Symbol/definition	Equation number
Energy	$E(k) = \frac{\hbar^2 k^2}{2m}$	(A.1)
Supply function	$f_0(k) = (m/\pi\beta\hbar^2)\ln\{1 + \exp[\beta(\mu - E(k))]\}$	(A.2)
Current density	$J(F) = \frac{1}{2\pi}\int_0^\infty \frac{\hbar k}{m} T(k) f_0(k)\mathrm{d}k$	(A.3)
Fermi–Dirac integral	$F_{1/2}(y) = \int_0^\infty \frac{\sqrt{x}}{1+e^{x-y}}\mathrm{d}x$	(A.4)
FNE g-function	$g(\mu,\beta,F) = \sum_{j=1}^\infty \frac{(-1)^j}{j\left(j+\frac{c_{\mathrm{fn}}}{\beta}\right)} e^{-j\beta\mu}$	(A.5)
WKB G-integral	$G(z) = \int_0^{\pi/2} \frac{\cos^2(s)\sin^2(s)}{\sqrt{z+\sin^2(s)}}\mathrm{d}s$	(A.6)
FNE v-function	$v(y) = 3(1-y^2)^{3/4} \times G\left(\frac{1}{2}\left(\frac{1}{\sqrt{1-y^2}} - 1\right)\right)$	(A.7)
FNE t-function	$t(y) = \left(1 - \frac{2}{3}y\frac{\mathrm{d}}{\mathrm{d}y}\right)v(y)$	(A.8)
FNE terms	$a_{\mathrm{fn}} = \frac{1}{16\pi^2\hbar\Phi t(y)^2}$; $b_{\mathrm{fn}} = \frac{4}{3\hbar}\sqrt{2m\Phi^3}v(y)$; $c_{\mathrm{fn}} = \frac{2}{\hbar F}\sqrt{2m\Phi}t(y)$	(A.9)

References

[1] Gilmour Jr AS. Microwave Tubes. Norwood MA: Artech House; 1986.
[2] Parker RK. Vide Sci Tech Appl 1996;52:366.
[3] Jensen KL, Lau YY, Levush B. Migration and escape of barium atoms in a thermionic cathode. IEEE Trans Plasma Sci 2000;28:772.
[4] Shih A. Private communication.
[5] Jensen KL. Field emitter arrays for plasma and microwave source applications. Phys Plasm 1999;6:2241.
[6] Zaidman EG, Kodis MA. Emission gated device issues. IEEE Trans Electron Dev 1991;38:2221.
[7] Kodis MA, Jensen KL, Zaidman EG, Goplen B, Smithe DN. IEEE Trans Plasma Sci 1996;24:970.
[8] Whaley DR, Armstrong CM, Gannon B, Mukhopadhyay-Phillips P, Spindt CA, Holland CE. PPM focused TWT using a field emitter array cold cathode. 1999 IEEE International Conference on Plasma Science (ICOPS), 1999 June 20–24; Monterey, CA, 6D01-02.
[9] Calame JP, Gray HF, Shaw JL. J Appl Phys 1993;73:1485.
[10] Whaley DR, Gannon B, Smith CR, Armstrong CM, Spindt CA. Application of field emitter arrays to microwave power amplifiers. IEEE Trans Plasma Sci 2000; 28:727.
[11] Bandy SG, Green MC, Spindt CA, Hollis MA, Palmer WD, Goplen B, Wintucky EG. Vacuum Electronics Annual Review Abstracts, New York: Palisades Institute for Research Services; 1997.
[12] Bandy SG, Green MC, Spindt CA, Hollis MA, Palmer WD, Goplen B, Wintucky EG. Conference Digest of the 11th International Vacuum Microelectronics Conference, 1998 July 19–24, Ashevile, NC. p. 132.
[13] Dayton JA, Hollis MA, Jensen KL, Murphy RA, Parameswaran L, Wintucky E. Private communication.
[14] Jensen KL, Abrams RH, Parker RK. J Vac Sci Technol B 1998;16:749.
[15] McGregor DS, Lau YY, Jensen KL. PAFED driven RF amplifier. Provisional Patent Application, January 12, 2000.
[16] Jensen KL. An analytical model of an emission-gated Twystrode using a field emitter array. J Appl Phys 1998; 83:7982.
[17] Modinos A. Field, thermionic, and secondary electron spectroscopy. New York: Plenum; 1984.
[18] Haas GA, Thomas RE. Thermionic emission and work function. In: Bunshah RF editor. Techniques of Metals Research, vol. VI, Part 1. New York: Wiley; 1972.
[19] Kubo R, Ichimura H, Usui T, Hashitsume N. Statistical mechanics. New York: North-Holland; 1965. p. 241.
[20] Jensen KL. Improved Fowler–Nordheim equation for field emission from semiconductors. J Vac Sci Technol B 1995;12:516.
[21] Flügge S. Practical quantum mechanics. New York: Springer; 1974 [see in particular problems 169 and 170].
[22] Lang ND, Kohn W. Theory of metal surfaces: charge density and surface energy. Phys Rev B 1970;1:4555.
[23] Lang ND. In: Ehrenreich H, Seitz F, Turnbull D, editors. The density-functional formalism and the electronic structure of metal surfaces, Solid State Physics. vol. 28, New York: Academic Press; 1973. p. 225–300.
[24] Kiejna A, Wojciechowski KF. Metal surface electron physics. Oxford: Pergamon; 1996.
[25] Jensen KL. Exchange-correlation, dipole, and image charge potentials for electron sources: temperature and field variation of the barrier height. J Appl Phys 1999;85:2667.
[26] Jensen KL. Errata: Exchange-correlation, dipole, and image charge potentials for electron sources: temperature and field variation of the barrier height. J Appl Phys 2000;88:4456.
[27] Forbes RG. Use of a spreadsheet for Fowler–Nordheim equation calculations. J Vac Sci Technol B 1999;17:534.
[28] Kittel C. Introduction to solid state physics. Fifth ed. New York: Wiley; 1976.
[29] Sze SM. Physics of semiconductor devices. Second ed. New York: Wiley; 1981.
[30] Jensen KL, Ganguly AK. Numerical simulation of field emission and tunneling: a comparison of the Wigner function and transmission coefficient approaches. J Appl Phys 1993;73:4409.
[31] Jensen KL, Ganguly AK. Numerical simulation of field emission from silicon. J Vac Sci Technol B 1993; 11:371.
[32] Jensen KL. Simulation of time-dependent quantum transport in field emission from semiconductors: complications

due to scattering, surface density, and temperature. J Vac Sci Technol B 1995;13:505.

[33] Lang ND, Kohn W. Theory of metal surfaces: induced surface charge and image potential. Phys Rev B 1973; 7:3541.

[34] Ancona MG. Density-gradient analysis of field emission from metals. Phys Rev B 1992;46:4874.

[35] Forbes RG, Jensen KL. Extension of the Fowler–Nordheim equation beyond the linear field + classical image charge potential approximation. Unpublished.

[36] Jensen KL. The semiconductor statistical hyperbolic/ellipsoidal model for evaluation of current from microstructures. 2000 Oct 22–27; Symposium II Proceedings of the Electrochemical Society, Phoenix, AZ. In press.

[37] Wen HJ, Ludeke R. Current oscillations in thin metal-oxide–semiconductor structures observed by ballistic electron emission microscopy. J Vac Sci Technol B 1998; 16:2296.

[38] Jensen KL, Mukhopadhyay-Phillips P, Zaidman EG, Nguyen K, Kodis MA, Malsawma L, Hor C. Appl Surf Sci 1997;111:204.

[39] Temple D, Palmer WD, Yadon LN, Mancusi JE, Vellenga D, McGuire GE. Silicon field emitter cathodes: fabrication, performance, and applications. J Vac Sci Technol A 1998; 16:1980.

[40] Filip V, Nicolaescu D, Okuyama F, Plavitu CN, Itoh J. Transport phenomena related to electron field emission from semiconductors through thick oxide layers. J Vac Sci Technol B 1999;17:520.

[41] Levine JD. Benefits of the lateral resistor in a field effect display. J Vac Sci Technol B 1996;14:2008.

[42] Ridly BK. Quantum processes in semiconductors, 2nd ed. New York: Oxford University Press; 1998 [see Fig. 3.21 p. 129].

[43] Jensen KL, Lau YY, McGregor D. Analysis of a photon assisted field emission device. Appl Phys Lett 2000;77:585.